Progress In Electromagnetics Research, PIER 68, 197–228, 2007

EFFECT OF WILDFIRE-INDUCED THERMAL BUBBLE ON RADIO COMMUNICATION

K. Mphale

Physics Department
University of Botswana
P/Bag 0022, Gaborone, Botswana

M. Heron

Marine Geophysical Laboratory
James Cook University
Townsville Q4811, Australia

T. Verma

Physics Department
University of Botswana
P/Bag 0022, Gaborone, Botswana

Abstract—Horizontal roll vortex pairs are dynamical structures that transfer energy and emissions from wildfires into the atmosphere. The vortices form at the edges of an intense line wildfire and emulate two cylinders, which form two curvatures of a biconcave thermal lens. Wildfire plume provides a dielectric material for the dielectric lens, whose permittivity is influenced by the nature, quantity of constituents (e.g., potassium and graphitic carbon) and variation of temperature with height in the plume. The environment created by the plume is radio sub-refractive with an effect of spreading radio wave beams. A numerical experiment was carried out to quantify loss of Ultra High Frequency (UHF) radio signal intensity when high intensity wildfire-induced horizontal roll vortices intercept UHF propagation path. In the numerical experiment, a collimated radio wave beam was caused to propagate along fuel-fire interface of a very high intensity wildfire in which up to two roll vortex pairs are formed. Maximum temperature of the simulated wildfire was 1200 K. Flame potassium content was varied from 0.5–3.0%. At 3.0% potassium content, a vortex pair imposed a maximum radio ray divergence of 2.1 arcmins while two vortex

pairs imposed a maximum divergence of 4.3 arcmins at the fuel-fire interface. The ray divergences caused maximum signal strength loss (in decibels (dB)) per unit path length of $0.154\,\mathrm{dBm}^{-1}$ and $1.65\,\mathrm{dBm}^{-1}$ respectively.

1. INTRODUCTION

Combustion in wildfires is often an incomplete process which gives out water vapour (H_2O) and carbon dioxide (CO_2) along with a large number of by-products in a smoke column [22]. The by-products consist of long list of chemicals which primarily include: carbon monoxide (CO), soot or black carbon (BC), inorganic particulates (e.g., K^+, Cl^-), and non-methane hydrocarbons (NMHC) [43]. The nature of the emissions is a factor of both fuel and meteorological conditions during the combustion. The emissions impact negatively on global climate, atmospheric visibility and human health: the gases, e.g., SOx and NOx, pollute the troposphere; carbon particles absorb and reflect solar radiation, therefore interfere with global solar energy budget; CO_2 and H_2O are green house gases, increased level of the gases leads to global warming; and fine particulate matter less than $2.5\,\mu$m (PM2.5) cause tract and lung infections such as acute respiratory infection [12]. During a wildfire, a large amount of heat energy is released into the atmosphere. The released energy is strong enough to drive atmospheric dynamics over a wide range of spatial scales [44]. On short temporal scale, heat released and emissions from wildfires create a sub-refractive environment for radio wave propagation.

Extensive high intensity wildfires often occur under windy and unstable atmospheric conditions [34]. Under these conditions, energy transfer from wildfires to the atmosphere is by forced convection. Towering smoke columns are buoyancy-induced fire thermals which are loaded with the emissions [20]. Initially, when a fire thermal breaks free from the surface air mass, there is tendency of air from a cooler layer aloft to move downwards so that it replaces ascending warm air. This initiates circular motion around the thermal bubble. On its ascension into the atmosphere, the warm air inside the bubble is acted upon by resistive frictional forces which cause it to roll backwards either side of the thermal centerline. The diverted air follows the path of cooler air from aloft which forms counteracting ring vortices. The roll vortices have been observed and simulated in wildfires under light to moderate windy conditions [17, 18, 10]. The vortices' air flow pattern is such that it entrains emissions, ambient air and surrounding materials into smoke column making the fire thermal dense at the centerline and diffused at

its periphery [8, 32]. The entrained heated material between the roll vortices creates a radio ray diverging biconcave thermal lens.

Vegetation contains Alkali and Alkaline Earth Metal (AAEM) species as part of the inherent inorganic ash. The AAEMs are mainly salts of potassium, calcium and sodium which exist in different physical forms, with the species of the potassium being a larger fraction of inorganic ash. AAEMs can exist; ionically or organically attached to oxygen-containing functional groups (i.e., O-C-) of the organic structure of plants, as discrete particles in voids of the organic matrix and in solution form such as in xylem vessels. During a wildfire, AAEMs are released from a thermally crumbling plant structure and convectively drawn into the combustion zone. As potassium species form a larger fraction of the omnipresent inorganic particulates in plants, they have been observed to form a large fraction of inorganic emissions during vegetation combustion [43, 27]. Wildfire combustion zone is characterized by high enough temperatures to cause thermal dissociation and ionization of AAEMs. Adiabatic wildfire flame temperatures range from 1900–2000°C [6, 40]. Alkali (e.g., K and Na) species have low dissociation energies (e.g., 3.79 eV for K_2CO_3) and low ionization potential (e.g., 4.34 eV for K). From studies of nutrient cycling, up to 28% of inherent potassium in plants is volatilized at combustion efficient of 98% [31]. Vodacek et al., 2003 also estimated that 10–20% of potassium in vegetation is ionized in wildfires. This creates a weakly ionized environment in the combustion zone.

The weakly ionized high temperature environment together with the emissions in the smoke creates a radio sub-refractive environment for radio wave propagation. The gases have dipole moments and the ability to be polarized by an impressed electric field. The combined effect of polarization and ionization is to refract radio wave signals from their propagation path [37]. The bending causes a significant radio signal path loss over long propagation distances [4].

2. WILDFIRE PLUME

2.1. Structure of a Wildfire Plume

There are three regions in a wildfire plume which are dynamically and physically distinct. The distinction lies in how temperature, plume velocity and implicitly dielectric permittivity vary in the regions. These regions are the: continuous and intermittent flames and the smoke column [24] and are as shown in Fig. 1. There is an immense literature on the behavior of these regions more especially the continuous flame and the smoke column regions [41, 29, 35]. Most of the literature on the continuous flame region concerns its intensity (I),

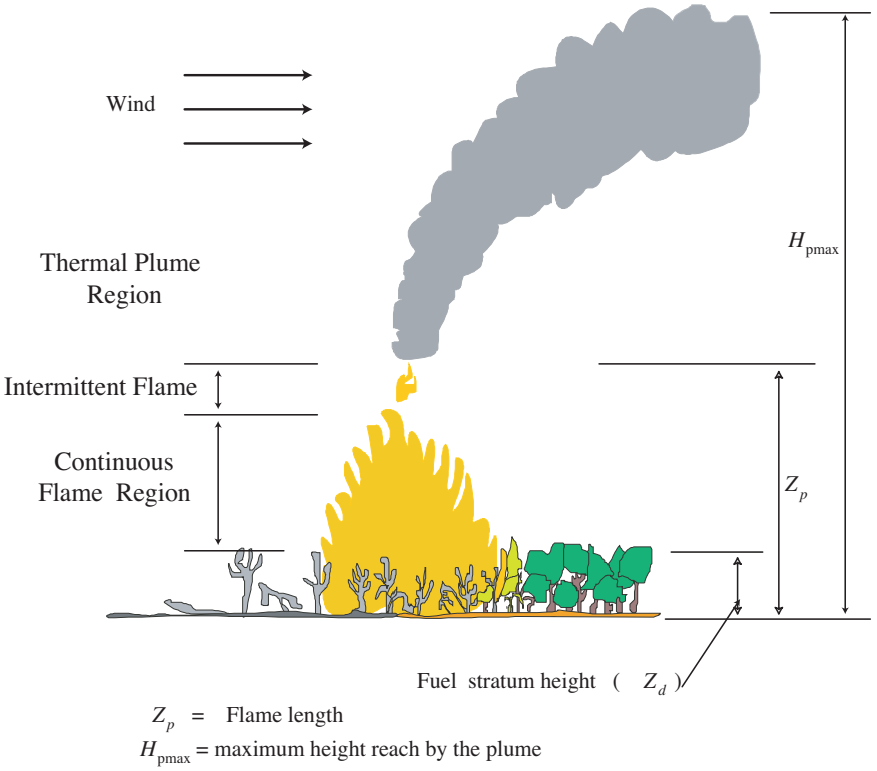

Figure 1. Vegetation fire plume in a slight wind.

rate of spread (RoS) under various conditions, velocity and thermal properties. The appreciation of these flame properties is in their relevance to fire suppression and firefighter safety. Very few people have studied the physical properties of intermittent region though [24]. There is lack of interest for the region among fire management scientists because its properties do not directly relate to a safety concern.

2.2. Properties of Wildfire Plume Regions

2.2.1. Wildfire Flame Model

Temperature variation in flaming region of the plume has been documented [35, 39]. According to [39], [45] gave an empirical relation that describes experimental data on temperature-time variation in the wildfire front with a fair amount of accuracy. The relation is a Rayleigh Distribution fit of the temperature-time curve. [45] gave the relation

as:

$$T_{fl} = T_{amb} + \frac{\alpha\beta}{\sigma} \exp\left\{ - \left[\frac{\beta}{\sigma} \right]^2 \right\} \tag{1}$$

where α and β are empirically determined constants and σ is distance from arbitrary origin.

Heat radiated from the flame of a propagating wildfire warms up the air ahead. The energy causes air temperature to decrease exponentially from a maximum value (T_{fl}) at the flame-fuel interface to the ambient (T_{amb}) some distance away in front of the flame. [7] modeled this exponential decrease in air temperature as:

$$T_{air} = T_{amb} + (T_{fl} - T_{amb}) \exp\left\{ - \left[\frac{x}{\lambda_d} \right] \right\} \tag{2}$$

where x and λ_d are distance from the bushfire front and gas temperature characteristic distance. Vertical temperature variation in the continuous flame above fuel layer decreases exponential with height. The decrease in temperature with height in the fire plume is given by [35] as:

$$T_{fl} = T_{\infty} + K \exp\left\{ \left(-\alpha_f (z - z_d)^2 \right) \right\} \tag{3}$$

where K, Z_d, Z_p are empirical constant, constant related to fuel height, constant related to flame height respectively and $\alpha_f = 1/\left(2z_p(z_p - z_d)\right)$.

Maximum temperature in both the vertical and horizontal sense occurs at about the center of the wildfire. Visible flaming edges are at lower temperature of about 600 K [11] than at the combustion zone, which can be up to 1300°C [5]. This produces temperature gradients between the edges and fire center. The temperature gradient causes a flow of ambient air into the flame, a process that lowers the adiabatic flame temperature (1900°C) by turbulent mixing to about a 1000°C.

High wildfire temperatures could lead to excitation and ultimately ionisation of flame constituents by two mechanisms; chemi-ionisation and thermal ionisation [23]. Methyl radicals (CH) exist in appreciable amounts in flames. Their encounter with high energy oxygen atoms in the flame could lead to chemi-ionisation of the radicals. However, it is less likely that oxygen atoms could exit in wildfires at normal temperatures of 1000°C in appreciable amounts for chemical ionisation to dominate. Alkalis such as sodium and potassium also exist in the flame in sufficient quantities to cause appreciable ionisation. Low ionisation potentials of the alkalis coupled with their high content of up 3.4% [30] in plant matter make thermal ionisation a predominant ionisation mechanism in wildfires.

2.2.1.1. Thermal Ionization in a Wildfire

During pyrolysis of vegetative matter, volatiles which contain AAEMs are released from plant's organic matrix and swept by convective currents into the combustion zone of flames. The most important of the AAEM species for thermal ionization are are potassium and sodium. The alkali atoms have low ionization potentials of 4.34 and 5.14 eV respectively. When the alkalis are released from the plant's structure as molecules they are thermally dissociated first and then ionized thereafter. Little heat is needed to dissociate alkali molecules e.g., dissociation energy of potassium salts range from as low as 0.75 eV to about 4.51 eV (for potassium chloride molecule). Potassium hydroxide (KOH) and sodium chloride (NaCl) have dissociation energy of about 3.51 and 4.24 eV respectively. The dissociation energy could be much less for complex organic salts of alkalis such as *malates* or oxalates. Number concentrations of singly ionized and neutral particles in the fire may depend on disassociation of the volatilized diatomic and polyatomic molecules according to the following relation;

$$AB(g) \rightleftharpoons A(g) + B(g) \tag{4}$$

where: $AB(g)$ is pyrolysate parent molecule; and $A(g)$, $B(g)$ are daughter particles.

Assuming local thermal equilibrium in the flame, the number concentration of dissociated particles can be determined by using Guldberg-Waage law. [21] gave the law as:

$$\frac{N_A N_B}{N_{AB}} = \frac{P_{Aint} P_{Bint}}{P_{ABint}} \left(\frac{2\pi kT}{h^2}\right)^{3/2} \left(\frac{m_A m_B}{m_{AB}}\right)^{3/2} \exp\left(\frac{-E_d}{kT}\right) \tag{5}$$

where: N_A, N_B and N_{AB} are number concentration of A, B and AB respectively; P_{Aint}, P_{Bint} and P_{ABint} are internal partition function of $A(g), B(g)$ and $AB(g)$; E_d is dissociation energy; k is Boltzmann constant; h is Planck constant; m_A, m_B, m_{AB} are masses of particles; and T is thermodynamic temperature.

Intense heat in the combustion zone electronically excite dissociated atoms such as A (see Eq. (4)) making them very unstable, thus giving atoms in the state A^*. On collision with other flame species (Fs) the atoms they give out their outer shell electron to produce singly ionized particles (A^+). Reaction Eq. (6) gives an account of ionization of excited atoms on collision with species Fs (see [3]);

$$Fs(g) + A^*(g) \rightleftharpoons A^+(g) + e^-(g) + Fs(g) \tag{6}$$

The overall equation for Eq. (6) is:

$$A(g) \rightleftharpoons A^+(g) + e^-(g) \tag{7}$$

Similarly, an equation that represents the ionization of diatomic species such NO in the flame is given by [21] as;

$$AB(g) \rightleftharpoons AB^{+}(g) + e^{-}(g) \tag{8}$$

To quantify the amount of ionization due to thermal ionization of alkalis and the composition of the flame, the application of Saha and Guldberg-Waage equations is sufficient as long as the flame is assumed to be in LTE. [21] gave the equation as:

$$\frac{N_{m^+}N_e}{N_m} = \frac{2P_{m^+int}}{P_{mint}}\left(\frac{2\pi \cdot m_e kT}{h^2}\right)^{3/2} \exp\left(\frac{-(E_i)}{kT}\right) \tag{9}$$

where: N_m, N_e and N_m are number concentration of singly ionized particles, electrons and neutral particles respectively; P_{mint} and P_{m^+int} are internal partition function of particles; E_i, and m_e are ionization energy and mass of an electron. The rest of the variables are as defined earlier.

Equation (9) is the ionization equilibrium constant (K_1). Electron density (N_e) due to thermal ionization of K atoms is related the ionization equilibrium constant and the total number of ionised K particles (N_p) in the flames as [13];

$$N_e = (K_1 N_p)^{1/2}\left[\left(1 + \frac{K_1}{4N_p}\right)^{1/2} - \left(\frac{K_1}{4N_p}\right)^{1/2}\right] \tag{10}$$

The total number of ionised K particles (N_p) is related to the potassium atoms in the flame by the equation;

$$N_p = \frac{7.335 \cdot 10^{21}\eta}{T}\,\mathrm{cm}^{-3} \tag{11}$$

where η is the number density of K atoms into the wildfire flame.

2.2.1.2. Wildfire Attenuation and Phase Constants

At microscopic scale, electrons appear to be in random motion. However, at macroscopic scale electrons have a directed motion, a drift in the direction of the impressed electric field. If the applied electric field and the thermal energy are not high enough to deviate the energy distribution from Maxwellian as is the case with wildfires, then equation of motion for an average electron in the slightly ionized gaseous medium undergoing repetitive collisions is given as;

$$m\ddot{d} + mv_{eff}\dot{d} = q_e\left[\vec{E} + \frac{\dot{d}}{c} \wedge \vec{B}\right] \tag{12}$$

Where $\dot{d}$ and $\ddot{d}$ are the drift velocity and acceleration of an average electron; $\vec{E}$ and $\vec{B}$ are electric and magnetic field vectors; c, m and q_e are speed of light, mass and charge of an electron charge; and v_{eff} is the effective momentum transfer collision frequency. The right-hand side of Equation (2) is Lorentz electromagnetic force. The contribution of $\vec{B}$ in the Lorentz force is so small that it can be neglected.

To solve equation for $\dot{d}$, $\vec{E}$ and $\dot{d}$ are assumed to vary as $e^{i\omega t}$ such that $\vec{E} = E_0 e^{i\omega t}$ and similarly for $\dot{d} = \dot{d}_0 e^{i\omega t}$. We then have,

$$\dot{d} = \frac{q_e}{m(v_{eff} + i\omega)}\vec{E} \tag{13}$$

The following relation relates the drift velocity of an average electron to the current density ($\vec{J}$); $\vec{J} = N\dot{d}q_e$. Where; N is the electron density.

Also $\vec{J} = \sigma\vec{E}$, this gives electric conductivity of the weakly ionized flame as;

$$\sigma = \frac{Nq_e^2}{m(v_{eff} + i\omega)} = \sigma_r + i\sigma_i \tag{14}$$

Equation (13) is a complex function with real part:

$$\sigma_r = \frac{\varepsilon_0\omega_p^2 v_{eff}}{(v_{eff}^2 + \omega^2)} \tag{15}$$

And the imaginary part;

$$\sigma_i = -\frac{\varepsilon_0\omega_p^2\omega}{(v_{eff}^2 + \omega^2)} \tag{16}$$

where; $\omega_p^2 = \left(\frac{Ne^2}{m\varepsilon_0}\right)$, ε_0 are the plasma collision frequency and free space permittivity.

Flame propagation constant is a measure of the rate of electromagnetic energy loss through the attenuation index and wave dispersion through the refractive index. Attenuation and refractive indices are dependent on the collision frequency and the electron density of a wildfire. These physical quantities can be determined from complex dielectric permittivity of the flame.

The dielectric permittivity for a wave in an ionized gas is given as

$$\varepsilon_r = 1 + \frac{\sigma_r}{i\omega\varepsilon_0} + \frac{\sigma_i}{\omega\varepsilon_0} \tag{17}$$

Substituting (14) and (15) into (16) gives

$$\varepsilon_r = \left[1 - \frac{\omega_p^2}{(v_{eff}^2 + \omega^2)}\right] - i\left[\frac{\omega_p^2 v_{eff}}{\omega(\omega^2 + v_{eff}^2)}\right] \tag{18}$$

Propagation constant γ is however related to the dielectric permittivity constant by the following relation;

$$\gamma^2 = -\mu_0\varepsilon_0\omega^2\varepsilon_r \rightleftharpoons \gamma = i\frac{\omega}{c}\sqrt{\varepsilon_r} \tag{19}$$

Also γ can be written as;

$$\gamma = \alpha_f + i\beta_f \tag{20}$$

Where α_f and β_f are derived from Maxwell's equations for a wave $E = E_0 e^{-i\gamma x}$ as;

$$\alpha_f = \frac{\omega}{c}\left\{-\frac{1}{2}\left(1-\frac{\omega_p^2}{\omega^2+v_{eff}^2}\right)+\frac{1}{2}\left[\left(1-\frac{\omega_p^2}{\omega^2+v_{eff}^2}\right)^2 + \left(\frac{\omega_p^2}{\omega^2+v_{eff}^2}\frac{v_{eff}}{\omega}\right)^2\right]^{1/2}\right\}^{1/2} \tag{21}$$

$$\beta_f = \frac{\omega}{c}\left\{\frac{1}{2}\left(1-\frac{\omega_p^2}{\omega^2+v_{eff}^2}\right)+\frac{1}{2}\left[\left(1-\frac{\omega_p^2}{\omega^2+v_{eff}^2}\right)^2 + \left(\frac{\omega_p^2}{\omega^2+v_{eff}^2}\frac{v_{eff}}{\omega}\right)^2\right]^{1/2}\right\}^{1/2} \tag{22}$$

For frequency range from HF to UHF and considering that the wildfire flame is weakly ionized with electron densities up to $10^{16}\,\mathrm{m}^{-3}$ and highly collisional (collision frequency in the range of 10^{11}–$10^{12}\,\mathrm{s}^{-1}$), $v_{eff} \gg \omega > \omega_p$. Eqs. (23) and (24) within the frequency range and therefore reduce to:

$$\beta_f = \frac{\omega}{c}\left(1-\frac{\omega_p^2}{2v_{eff}^2}\right) \tag{23}$$

and

$$\alpha_f = \frac{\omega}{c}\left(-\frac{\omega_p^2}{2\omega v_{eff}}\right) \tag{24}$$

2.2.1.3. Radio Refractive Index for Wildfire Flame

Radio refractive index of a weakly ionized gas is related to incident radio wave's phase shift and attenuation per meter by the equation;

$$n_f = \frac{c}{\omega}\beta_f - i\frac{c}{\omega}\alpha_f \tag{25}$$

where $n_f, c, \omega, \beta_f, \alpha_f$ are refractive index of the flame, speed of light, phase and attenuation constants of an electromagnetic wave due to the flame. Equations (23) and (24) give complex refractive index (25) in the combustion zone of the wildfire plume as:

$$n_f = \left(1 - \frac{\omega_p^2}{2v_{eff}^2}\right) - i\left(\frac{\omega_p^2}{2\omega \cdot v_{eff}}\right) \tag{26}$$

2.2.2. Buoyant Smoke Plume Model

Wildfires liberate enormous amount of heat energy into the atmosphere by means of a smoke column [41]. Combustion products and aerosols are transported into the atmosphere through the convection column. Air from the surrounding atmosphere entrains into the column as it rises. The entraining air dilutes the smoke and makes it spread with height. Mercer et al. [25] developed a model that relates plume temperature, density, vertical and entrainment velocities to plume radius. The model's governing equations are derived from balancing mass, momentum and energy fluxes. Mercer et al.'s model assumes top-hat distribution of the variables, thus a variable such as velocity is assumed to be constant across a cross section perpendicular to the plume's centerline. From the conservation of thermal energy, [25] gave temperature variation in the convection column as:

$$\frac{d\left(\rho_p b w T_p\right)}{ds} = \rho_a v_e T_{amb} \tag{27}$$

where $\rho_a, \rho_p, T_{amb}, T_p, b, v_e$ and w are ambient air density, plume density, ambient temperature, plume temperature, plume radius, entrainment velocity and vertical velocity of the plume respectively.

Assuming ideal gas behavior of the plume, its density can be related by;

$$\rho_p = \rho_a \frac{T_{amb}}{T_p} \tag{28}$$

When Gaussian distribution is fitted on the top-hat data, it gives temperature distribution of the form [25]:

$$T_G = T_a + \frac{N}{\lambda^2}\left(T_p - T_a\right)\exp\left\{-\frac{r^2}{\lambda^2 b^2}\right\} \tag{29}$$

where $r, N,$ and λ^2 are radial distance normal to the centerline trajectory, plume edge criterion, which is usually taken to be 2 and spread ratio, also usually taken to be 1 respectively.

Weber et al. [35] also fitted a Gaussian distribution on the experiment data and gave the temperature-time variation in the plume to be in the form:

$$T' = \frac{A}{z} \exp\left(\frac{-t^2}{B^2 z^2}\right) \tag{30}$$

where z is height above the ground, A and B are empirically determined factors. Weber et al. [35] observed that (30) can be explicitly written as:

$$\Delta T = \frac{k I^{2/3}}{z} \exp\left(\frac{-x^2}{\beta^2 z^2}\right) \tag{31}$$

where A has been replaced with the product of fire-line intensity (I) to the power of $2/3$ and proportionality constant k. Entrainment constant (β) and horizontal distance (x) from the line source replace B and t respectively.

2.2.2.1. Radio Refractive Index for Wildfire Smoke

At radio wave frequencies up to 20 GHz, radio refractivity for unionized plume (air and smoke) is frequency independent but dependent on the constituents more especially water vapor [15]. A wildfire smoke is made up products of vegetation combustion, which are primarily water vapor (H_2O), carbon monoxide (CO) and carbon dioxide (CO_2). Nitrogen (N_2) from the air and other by-product of incomplete combustion form a significant portion of the mixture. Oxygen (O_2) is also present in significant quantities due to the entrainment of ambient air into the smoke plume as the column rises up into the atmosphere.

Polarizability (P) of a medium impressed upon by an electric field is given by Debye relation as (see [2]):

$$P(\omega) = \frac{4N_a\pi}{3}\left[\alpha_0 + \frac{\mu^2}{3kT}\left(\frac{1}{1+i\omega\tau}\right)\right] \tag{32}$$

where $\omega, \alpha_0, \mu, k, N_a, T$, and τ are electric field frequency, polarization factor for a plume gas, electric moment dipole of the plume gas, Boltzmann's constant, Avogadro's constant, plume temperature and relaxation time of the molecules to return to their random distribution after an impressed electric field is removed respectively.

Dielectric permittivity (ε) of a gas is related to polarizability by

$$P(\omega) = \left(\frac{\varepsilon - 1}{\varepsilon + 2}\right)\left(\frac{M}{\rho}\right) \tag{33}$$

where M and ρ are molecular weight and density of a gas.

Equating (32) and (33) gives

$$\frac{\varepsilon - 1}{\varepsilon + 2} = \frac{4N_a\pi\rho}{3M}\left[\alpha_0 + \frac{\mu^2}{3kT}\left(\frac{1}{1 + i\omega\tau}\right)\right] \tag{34}$$

At frequencies less than 100 GHz, $\omega\tau \ll 1$ [2] and for most gases, $\varepsilon + 2 \cong 3$, therefore (34) can be approximated to

$$\varepsilon - 1 = \frac{4N_a\pi\rho}{M}\left[\alpha_0 + \frac{\mu^2}{3kT}\right] \tag{35}$$

Assuming that air and smoke plume behave ideally, pressure of a specific volume is related to absolute temperature by the ideal gas equation,

$$P = \rho RT \tag{36}$$

Substituting (36) into (35) gives

$$\varepsilon - 1 = \frac{4N_a\pi P}{RT}\left[\alpha_0 + \frac{\mu^2}{3kT}\right] \tag{37}$$

A compact form of (37) will be

$$\varepsilon - 1 = \frac{k_{a/p}P}{T} \tag{38}$$

where $k_{a/p}$ is constant for the smoke plume.

As the smoke plume is composed of many gases, the constant $k_{a/p}$ can be broken down to account for each plume constituent, each having its own constant. Equation (37) can therefore be written as

$$\varepsilon - 1 = \sum_{1}^{r} \frac{k_{gr}P_{gr}}{T} \tag{39}$$

where k_{gr} and P_{gr} are constant for air or plume gas constituent and its partial pressure.

Permittivity (ε) is related to refractive index (n) by the relation: $\varepsilon - 1 = n^2 - 1$. Using binomial expansion, $\varepsilon - 1 \approx 2(n - 1)$.

Therefore (38) becomes,

$$n - 1 = \frac{2N_a\pi \cdot P}{RT}\sum_{1}^{r}\left[\alpha_{0r} + \frac{\mu^2}{3kT}\right] \tag{40}$$

Refractive index (n) of the smoke plume is then give by

$$n = 1 + \left\{\frac{2N_a\pi \cdot P}{RT}\sum_{1}^{r}\left[\alpha_{0r} + \frac{\mu^2}{3kT}\right]\right\} \tag{41}$$

3. WILDFIRE PLUME RADIO REFRACTIVE INDEX

3.1. Effective Radio Refractive Index of Wildfire Plume

Radio refractivity (N) is defined by ($(n-1)\times 10^6$). By this definition, refractivity in the combustion zone of the wildfire plume can be expressed as:

$$N_{\text{combustion zone}} = \left[-\frac{1}{2}\left(\frac{\omega_p^2}{v_{eff}^2}\right) - i\left(\frac{\omega_p^2}{2\omega v_{eff}}\right)\right]\cdot 10^6 \tag{42}$$

And refractivity in the smoke plume can also be given as:

$$N_{\text{smoke plume}} = \left\{\frac{2\cdot N_a\pi\cdot P}{RT}\cdot\sum_1^r\left[\alpha_{0r}+\frac{\mu_r^2}{3kT}\right]\right\}\cdot 10^6 \tag{43}$$

The refractivities for the two region of the fire plume (i.e., Eqs. (42) and (43)) add to give effective refractivity ($N_{\text{effective}}$) of wildfire at any point of the plume. The effective refractivity of the plume is then given as:

$$\begin{aligned} N_{\text{effective}} &= \left\{\left[\frac{2\cdot N_a\pi\cdot P}{RT}\cdot\sum_1^r\left[\alpha_{0r}+\frac{\mu_r^2}{3kT}\right]\right.\right. \\ &\quad \left.\left.-\frac{1}{2}\left(\frac{\omega_p^2}{v_{eff}^2}\right)\right] - i\left[\frac{\omega_p^2}{2\omega v_{eff}}\right]\right\}\cdot 10^6 \end{aligned} \tag{44}$$

From the definition of refractivity, effective complex refractive index ($\tilde{n}_{eff}$) of wildfire plume is given as:

$$\begin{aligned} \tilde{n}_{eff} &= \left\{\left[1+\frac{2\cdot N_a\pi\cdot P}{RT}\cdot\sum_1^r\left[\alpha_{0r}+\frac{\mu_r^2}{3kT}\right]\right.\right. \\ &\quad \left.\left.-\frac{1}{2}\left(\frac{\omega_p^2}{v_{eff}^2}\right)\right] - i\left[\frac{\omega_p^2}{2\omega v_{eff}}\right]\right\} \end{aligned} \tag{45}$$

Magnitude of the complex refractive index ($\tilde{n}_{mag}$) is then calculated from (45) as:

$$\begin{aligned} \tilde{n}_{mag} &= \left\{\left[1+\frac{2\cdot N_a\pi\cdot P}{RT}\cdot\sum_1^r\left[\alpha_{0r}+\frac{\mu_r^2}{3kT}\right]\right.\right. \\ &\quad \left.\left.-\frac{1}{2}\left(\frac{\omega_p^2}{v_{eff}^2}\right)\right] + \left[\frac{\omega_p^2}{2\omega v_{eff}}\right]^2\right\}^{1/2} \end{aligned} \tag{46}$$

4. THERMAL BUBBLE IN A WILDFIRE

4.1. Initiation of Thermal Bubbles

The earth surface absorbs radiation from the sun and re-emits it in form of long waves into the atmosphere. The emitted long waves continually warms up the air near the ground surface with the consequence of troposopheric temperature decreasing with the increase in altitude (i.e., at the lapse rate, $\Gamma' = 0.65°\text{C}/100\,\text{m}$). Under normal atmospheric conditions, the mode of heat transfer from the surface air mass (SAM) to air mass directly above it (AAM) is by conduction when there are small but significant temperature gradients. Large temperature gradients have a potential to trigger convective heat transfer. Consider an air parcel in SAM with temperature T_s warmer than AAM, which is at T_a. Since SAM is warmer than AAM, it becomes lighter than AAM and therefore becomes buoyant and unstable. Specific buoyancy force on the air parcel (f_{buoyancy}) will be towards AAM with magnitude $g(T_s - T_a)/T_a$, where g is acceleration due to gravity. The buoyancy cause SAM to bulge upwards directly over the heat source and some of the cooler air in AAM will sink towards SAM (see Figure 2). Continuous heating of SAM causes the air to bulge into a bubble, which finally breaks away from the surface air mass to form a thermal bubble. The evolution of the thermal bubbles becomes vigorous when $(T_s - T_a)$ is large as it is the case with a wildfire.

A parameter that determines the onset of convective heat transfer in the atmosphere is the Rayleigh Number (Ra). Ra is a dimensionless ratio between the product of buoyancy forces and heat advection and the product of viscous forces and heat conduction in a fluid. It is given by Nikolaenko et al. [26] as:

$$Ra = \frac{g \cdot \alpha \cdot \Delta T \cdot L^3}{v \cdot \kappa} \tag{47}$$

where $g, \alpha, \Delta T, L, v$ and κ are acceleration of gravity, isobaric thermal expansion coefficient, temperature difference, characteristic length, kinematic viscosity and thermal diffusivity. This occurs when the Ra exceeds a critical value of 1708 (Ra_c). Values of $Ra < Ra_c$ favor the conduction as a mode of heat transfer.

4.2. Structure of Thermal Bubbles

As the thermal bubble ascends through the atmosphere its size increases with the decrease in atmospheric pressure. Convective up draughts push hot gaseous combustion products to the center of the bubble. This makes temperature and velocity highest at the centerline.

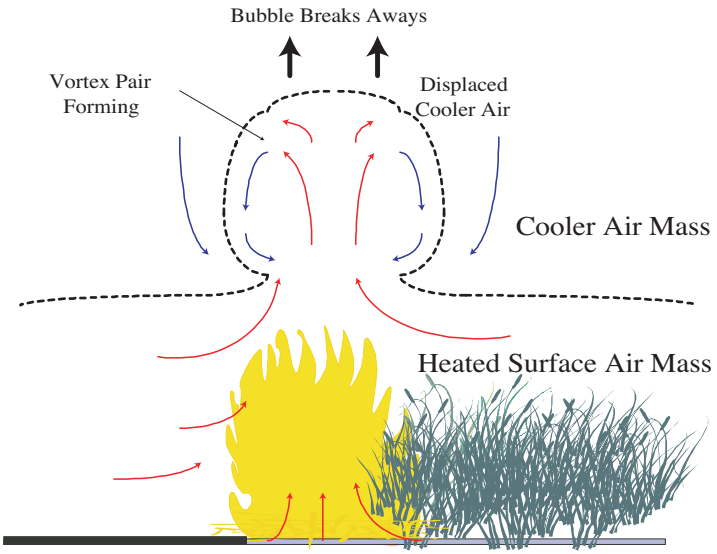

Figure 2. Initiation of a wildfire-induced thermal bubble.

Due to high velocity at the bubble centerline, internal buoyant forces produce vortex tubes that are circular rings concentric with the vertical axis (see [4, 8]. Depending on vertical potential temperature and velocity gradients in the bubble, the vortices can either be roll or cellular. This behavior is summed up in the bulk Richardson Numbers (Ri_b), a dimensionless quantity that relates vertical stability to vertical shear. Bulk Richardson Numbers (Ri_b) is given by [17] as:

$$Ri_b = \frac{g\left(d\overline{\theta}/dz\right)}{\overline{T}\left(d\overline{u}/dz\right)^2} \tag{48}$$

where $g, d\overline{\theta}/dz, d\overline{u}/dz$ and $\overline{T}$ are acceleration due to gravity, average potential temperature gradient, average velocity gradient and average fire temperature. According to [17], low values of Ri_b favor the generation of roll vortices while large values of Ri_b favor the cellular convection. Convective roll vortices such as those observed in crown fires has Ri_b values as low as -0.022 [16]. Figure 3 shows typical concentric vortex rings over a wildfire. As the vortices ascend to the atmosphere, they suck in cool atmospheric air along the plume periphery. The sucked in cool air mixes in a turbulent manner with the combustion products. This ultimately leads to loss of momentum in plume, buoyant forces losing their strength and finally the plume spreads as it rises.

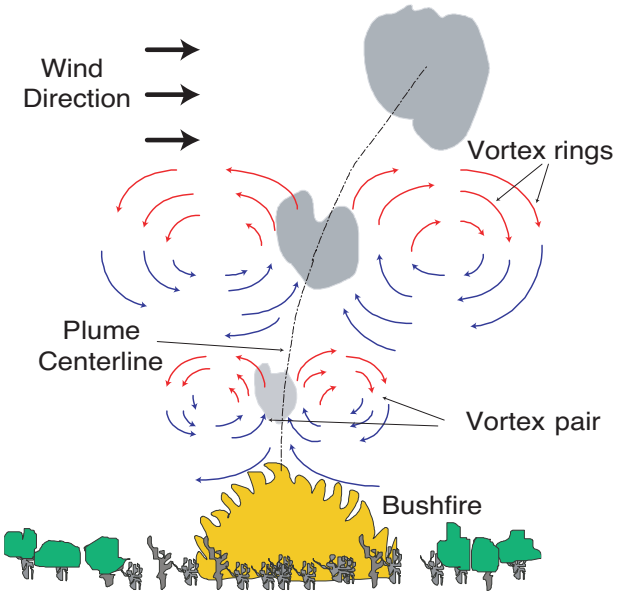

Figure 3. Horizontal roll vortices flanking an intense wildfire flame.

4.3. Occurrences of Roll Vortices in Wildfire Environments

The occurence of Roll Vortices (RV) in very high intensity bushfires and grass fires **has been documented (e.g., in [8, 6] and [46]. Vortices can exist as: Vertical Roll Vortices (VRV), which takes the form of fire-whirls; and Horizontal Roll Vortices (HRV). HRVs are a result of bending of VRV in light to moderate speed wind. The bending results in the reduction in angular velocity and loss of ferocity [46]. HRVs exist in at least three forms: longitudinal vortex pair, single longitudinal vortex and transverse roll vortex [17]. The most common HRV in bushfire environment is the longitudinal vortex pair, thus that which is shown in the thermal bubble. The longitudinal vortices are considered one of the ways by which crown fires spread; at least in coniferous forests [17].

The interaction of the plume with the winds creates vortex tubes that are bent and stretched along the flanks of the plume [8]. Counter rotating roll vortex pairs are then formed over the flaming area provided the wind speeds are light to moderate. Further downwind of the plume, strong vorticity and weak buoyancy effects may exist. The counter-rotational vortices that still exist in this region lie almost parallel to the surface.

4.4. Conditions for the Occurrence of HRV

At least three conditions are critical to the occurrence of HRVs. HRVs are hard to form in rough terrain as a result of complex airflow and turbulence [46]. High wind speed breaks up the roll vortices. Very high temperatures are very **important for the formation of the HRVs. This can be inferred from equations (47) and (48) in which high temperature gradient and high average temperature are very important for low Richardson and high Raleigh numbers respectively. This can be inferred from equations (47) and (48) in which high temperature gradient and high average temperature are very important for low Richardson and high Raleigh numbers respectively. This of course restricts the formation of HRVs to fire burning extreme bushfire weather. Roll vortices formed from crown fire are dependent on temperature gradient in the burning area. This causes a wind to flow transverse to the burning area, a very important component to the initiation of horizontal vortices. Light to moderate ambient wind of $6\,\mathrm{ms}^{-1}$ is a necessity for the formation of longitudinal pair and transverse vortices while single longitudinal vortices require winds up $22\,\mathrm{ms}^{-1}$.

Longitudinal vortex pair is the most common HRV in crown fires. They are considered the most common method by which crown fires spread. They create "crown streets" whenever they occur in a grassland or forests. Crown streets are rows of unburned vegetation, which remain after a crown fire. The crowns are saved by cool air in the descending arm of counter-rotational vortex pair (see Figure 3). The air circulation in the vortices drives fire in opposite directions so much that it is only the tree stems that are charred. The char heights are low and in opposite directions on either sides of the crown streets.

5. NUMERICAL EXPERIMENT

5.1. Biconcave Thermal Lens Model for Radio Wave Refraction

The horizontal vortices that form at the edges of an intense line bushfire emulate two cylinders, which form two curvatures of a biconcave lens (see Fig. 4). The wildfire plume provides a dielectric material for the lens configuration. Plume constituents and temperature variation influence the refractivity of the plume. The model considers the flame and the region up to 5 m round the flame to consist of emission gases H_2O, CO_2, CO and N_2 in the proportions given by [28] as (Table 1):

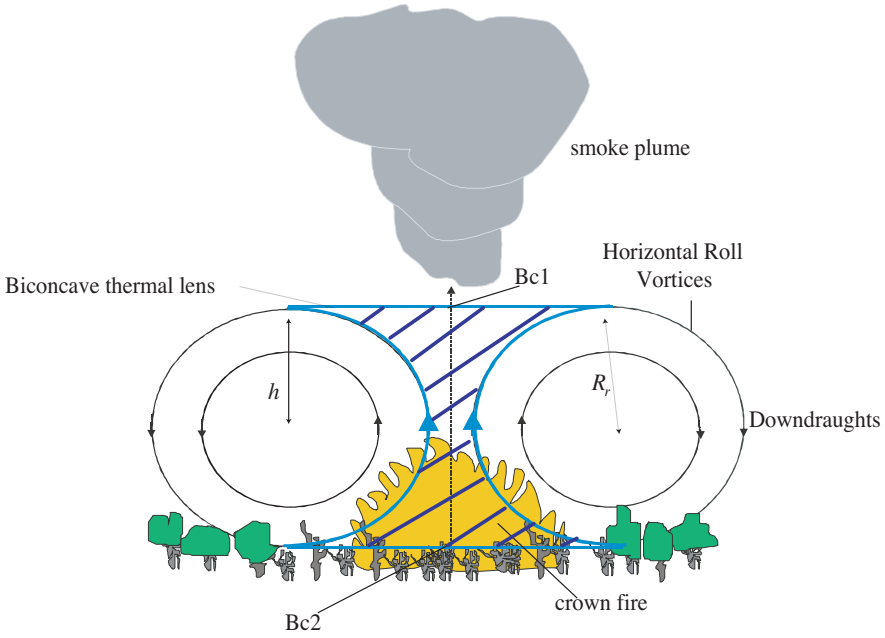

Figure 4. Thermal biconcave lens formed by horizontal roll vortices.

Table 1. Wildfire plume gas composition.

Gas:	H_2O	CO	CO_2	N_2
(% /v)	0.056	0.0024	0.025	0.703

5.2. Radio Ray Divergence by the Thermal Lens

The configuration of the vortices and the plume form a biconcave thermal lens (shaded in blue in Fig. 4). Its focal length is expected to be some kilometers away form the bushfire because the thermal lens is dielectrically "thin". According to the lens maker equation, the power of the vortex made lens $(1/f)$ is given by:

$$\frac{1}{f} = (\tilde{n}_{mag} - n_a)\left[\frac{1}{R_{r1}} + \frac{1}{R_{r2}}\right] \tag{49}$$

where n_a, R_{r1}, R_{r2} and f are radio refractive index of air, radius of curvature of a vortex and focal length of the lens respectively.

Assuming that the vortices are of the same radius, eq. (49) becomes

$$\frac{1}{f} = \frac{2(\tilde{n}_{mag} - n_a)}{R_{rc}} \tag{50}$$

where R_{rc} is the common radius for the both vortices. A typical radius for a vortex is 200 m e.g., Mack Lake crown fire [16]. In Geometrical optics, rays projected parallel to the principal axis to a bi-concave lens are diverged by angle (δ) related by

$$\delta = \tan^{-1}\left[\frac{h}{f}\right] \tag{51}$$

where h is the height relative to the principal axis of the lens.

However, the deviation angles are small, therefore Eq. (51) can be written as;

$$\frac{1}{f} = \frac{\delta}{h} \tag{52}$$

Equating Eqs. (50) and (52) gives;

$$\delta = \frac{2h(\tilde{n}_{mag} - n_a)}{R_{rc}} \tag{53}$$

The implication of Eq. (53) is that deviations are small at cooler parts of the thermal lens where $\tilde{n}_{mag}$ are close to n_a and high for the hottest part where $\tilde{n}_{mag}$ is less than n_a. For a thermal cell, the ratio of h and R_{rc} is approximately 1.6 [4], therefore Equation (53) can be simplified to:

$$\delta = 3.2 \times 10^6 \times |\tilde{n}_{mag} - n_a| \text{ (mrads)} \tag{54}$$

Radio refractive index of air at standard temperature and pressure is 1.000272 [4], therefore equation (54) can be written as:

$$\delta = 3.2 \times 10^6 \times |\tilde{n}_{mag} - 1.000272| \text{ (mrads)} \tag{55}$$

At a distance ξ from a thermal lens, a ray that propagates parallel to the lens' principal axis and diverted by angle δ after passing through the lens will be raised by a height, $\xi \tan\delta$. Assuming a narrow circular beam with radius r, signal strength loss (attenuation) at ξ (in dB) can be approximated by the relation:

$$\text{Signal Strength Loss (dB)} = 20\log_{10}\left(1 + \frac{\xi \tan\delta}{r}\right) \tag{56}$$

Angle of incidence is assumed to be close to zero. For a series of thermal lens intercepting the propagation path, Signal attenuation due to the two thermal lenses is given by [4] as:

$$\text{Signal Strength Loss (dB)} = \left(\frac{17.39\delta}{d \cdot \varphi}\right) \tag{57}$$

where d and φ are distance between the lenses and beam angle (taken as 0.05° for the experiment) respectively.

5.3. Application of the Thermal Lens Model to Mack Lake Crown Fire

The thermal lens model is applied to predict radio wave deviation in a crown fire that occurred in the Mack Lake in Huron National Forest, Michigan, USA [16]. The fire consumed 10040 ha of jack pine forest (height: 6–18 m). This created crown streets of 11 km long and maximum width of 200 m. The maximum distance between streets was observed to be 850 m. The behavior of the crown fire is as given in Table 2.

Table 2. Mack Lake crown fire behavior and horizontal roll vortex properties.

Range of RoS (m/s)	Range of Flame Height (m)	Range of Roll radius(m)	Range of Fireline Intensity (MWm^{-1})
0.04-3.14	10-25	11-200	1.83-103

5.3.1. Temperature-Height Variation in a Crown Fire

Temperature gradients that exist in the crown bushfire plume though complex can be modeled by appropriate equations in Section 2.2. Unlike when the fuel layer is thin, temperatures in the fuel stratum of a crown bushfire seems to rise steadily from a minimum value of about 300°C to a maximum value at near fuel-air interface within the fuel stratum. Beyond the fuel canopy, plume temperature falls exponentially with height until it reaches the ambient air temperature. To illustrate this, temperature data obtained during International Crown Fire Modeling Experiment (ICFME) for Plot 9 [5] is used. The data is from near ground level (3.1 m) to 13.2 m (above canopy). Beyond 13.2 m, an extrapolation of temperature was made using Weber

et al.'s relation (Eq. (3)). The temperature-height variation up to 22 m above ground level for the crown wildfire is shown in Fig. 5.

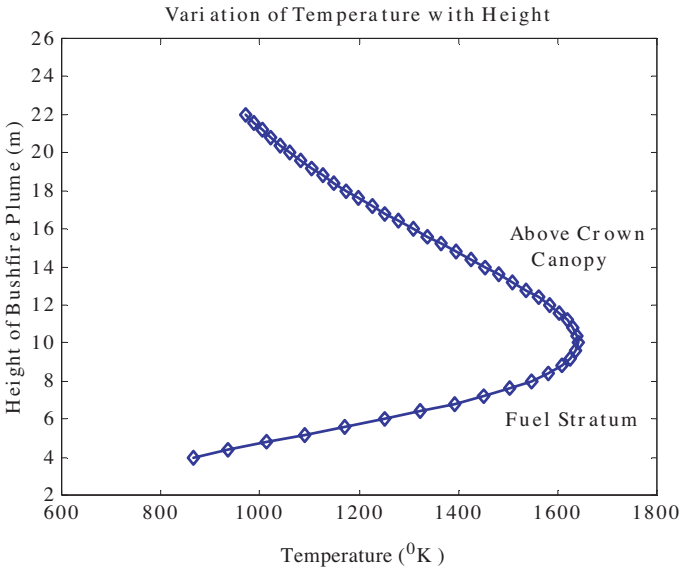

Figure 5. Temperature variation with height for a crown fire (adpt'd: [5]).

5.3.2. Refractive Index-Height Variation in the Crown Fire

Mack lake crown fire had a wide range of behavior, and ICFME's Plot 9-crown fire [5] is taken as a case study. Plot 9's fire-intensity was about 90 MWm^{-1}, RoS and observed flame heights were 1.16 m/s and 20–30 m respectively. An HRV radius of 20 m, a range of potassium content in the jack pine of 0.5–3.0% and fire behavior identical to that of Plot 9 are assumed and the refractive index of the thermal lens was calculated as per Eq. (45). The dipole moments and polarizabilities of plumes gases used in the calculation of refractive index are shown in Table 3. The variation of refractive index with height for the thermal is shown in Fig. 6.

Table 3. Dipole moments and polarizabilities of plume gases (adapted from [47] and [48]).

Combustion gas:	N_2	H_2O	CO	O_2	CO_2
Dipole Moment (μ_r) (Debye)	-	1.65[b]	0.112[b]	-	0.1[b]
Polarization Ability(α_{or})	1.76[a]-1.84[b]	1.5_b	1.95[a]-2.02[b]	1.6[a]	2.6[b]

a and *b* refer [47] and [48] respectively.

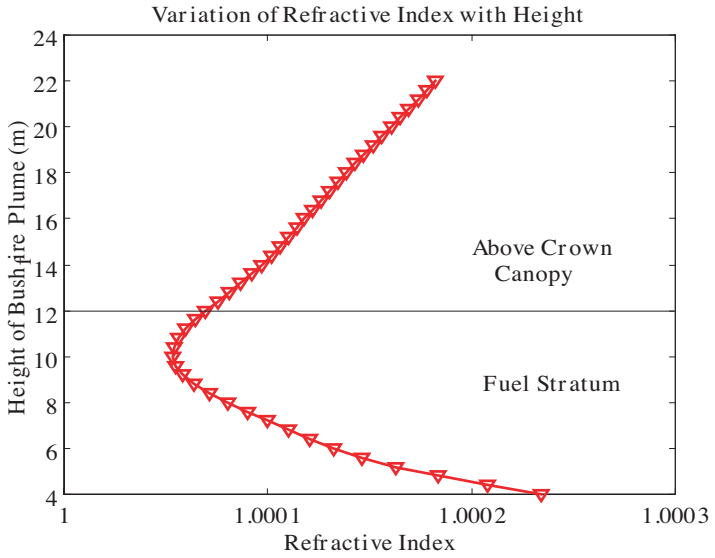

Figure 6. Refractive index variations with height for a crown fire.

6. NUMERICAL RESULTS AND DISCUSSIONS

6.1. Radio Ray Deviation for a Single Thermal Lens

The thin thermal lens model was run for a region 6–22 m above the ground surface. The model predicted radio ray deviation of 0.364–0.124 mrads for this region when 0.5% of the flame constituents is K. Maximum ray deviation of 0.622 mrads was observed at the hottest part of the wildfire, thus at 10 m above ground surface. The range of ray deviation when potassium content in the flame particulates is 3.0%

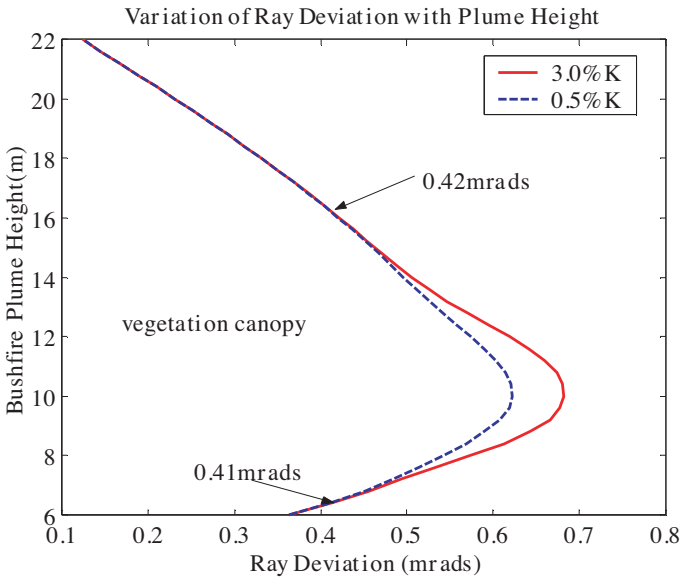

Figure 7. Variation of ray divergence with height at 0.5 and 3%K.

is same as that for K content is 0.5%. However, maximum deviation for 3.0%K which also occurs at 10 m above ground is 0.682 mrads. It could also be observed from Figure 7, that the effect of flame potassium content in ray deviation occurs between 6.37–16 m above ground in the wildfire plume.

6.2. Radio Ray Deviation for Double Thermal Lenses

When a collimated beam of radio rays is considered to propagate at grazing angle to the vegetation canopy i.e., along the fuel-flame interface, of which flame potassium content is 0.5%, ray deviation were observed to range from 1.97–0.43 arcmins for range 12–22 m above ground for a single lens (Fig. 8). The deviation is almost doubled to 3.95–0.85 arcmins for this region at the same potassium content when two thermal lenses of the same thermo-physical properties intercept the radio rays propagation path. When potassium content is increased to 3%, deviations were observed to range from 2.13–0.43 arcmins for the region 12–22 m above ground for a single thermal lens (Fig. 9). The deviations were also doubled to 4.25–0.43 arcmins for a double thermal lens configuration at 3%K.

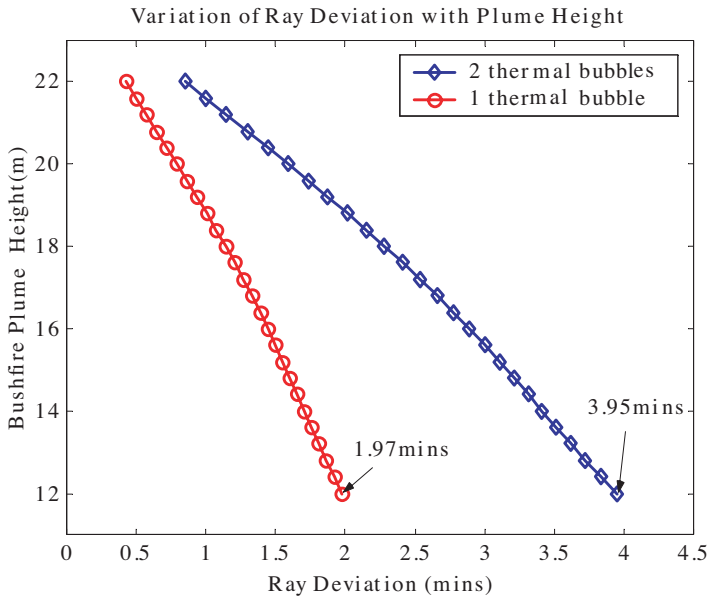

Figure 8. Variation of ray divergence with height for 1 and 2 thermal lenses at $0.5\%K$.

6.3. Radio Wave Attenuation Coefficient Due to Thermal Lenses with $0\%K$

A radio receiver for a collimated beam form a transmitter which is at the same level as the receiver suffers a signal loss when intercepted by a thermal lens. From the simulation, loss in signal strength per unit distance (dBm^{-1}) is observed to range from $0.151\,\mathrm{dBm}^{-1}$ at 12 m above ground to $0.136\,\mathrm{dBm}^{-1}$ at 22 m for a single thermal lens when there no potassium in the flame (Fig. 10). When there are two thermal lenses of the same thermo-physical properties intercepting the propagation path, signal strength loss per unit distance has been observed to range form 1.42–$0.33\,\mathrm{dBm}^{-1}$ for the region 12–22 m above ground respectively. The simulation results suggest that even if there is no potassium in the flame significant ionization is still observed; maximum at the hottest part of the flame and significantly less so at cooler parts of the flame. More than one thermal lens of the similar dielectric permittivity gradient exacerbated the signal strength loss effect and the effect is not a linear sum of attenuation coefficient at particular height.

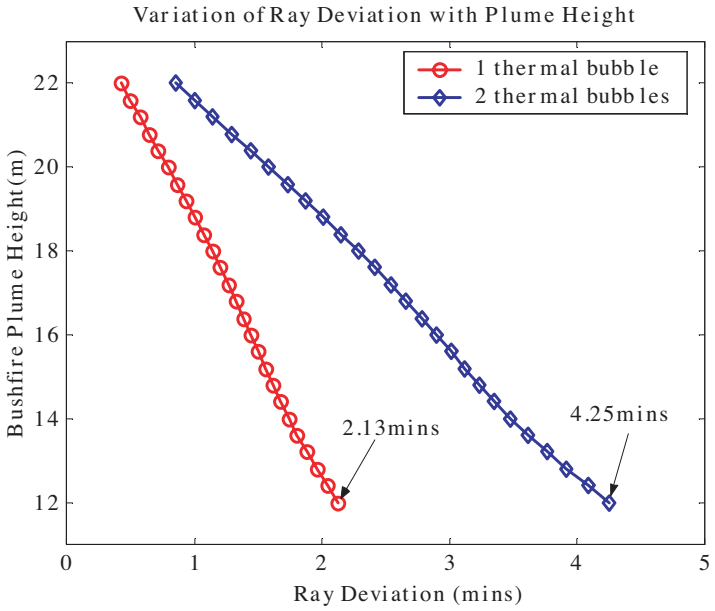

Figure 9. Variation of ray divergence with height for 1 and 2 thermal lenses at 3.0%K.

6.4. Radio Wave Attenuation due to a Single Thermal Lens

The contribution of ionization to the refractive index Equation (45) is limited to a height 16 m above ground level for a flame with 3%K content. The contribution is even less for a flame with 0.5%K; only up to 14.7 m above ground. The model estimates signal loss per unit distance that ranges from 0.152 dBm^{-1} at 12 m above ground to 0.136 dBm^{-1} at 22 m for potassium content of 0.5% in the flame (Fig. 11). At potassium content of 3.0%, signal strength loss per unit distance has been observed to range form 0.154–0.136 dBm^{-1} for the region 12–22 m above ground respectively. The simulation results suggest that even though heat energy at 22 m above ground is enough to ionize potassium, the ionization due to potassium content increase of 2.5% is not sufficient to make a significant change in radio refractivity at UHF. The attenuation coefficient decrease with the increase in wildfire plume height from a maximum of 0.24 dBm^{-1} at the combustion zone to a value 0 dBm^{-1} at a height when refractive index of the plume is equal to that air at standard temperature and pressure (1.000272).

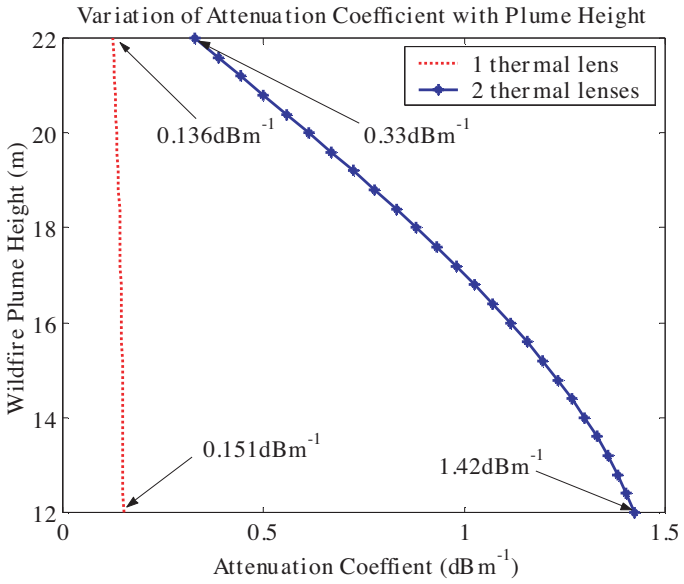

Figure 10. Attenuation coefficient vs. height for 1 and 2 thermal lenses for flames with $0\%K$.

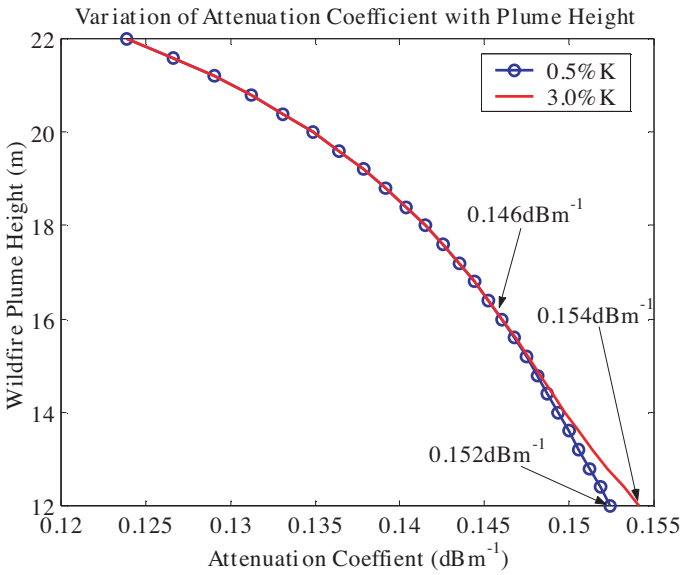

Figure 11. Attenuation coefficient vs. height for 1 thermal lens for flames with 0.5 and $3.0\%K$.

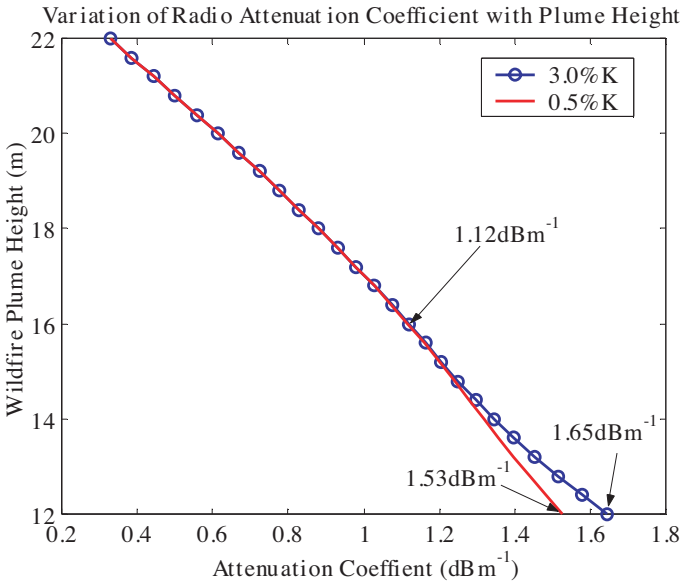

Figure 12. Attenuation coefficient vs. height for 2 thermal lenses for flames with 0.5 and 3.0%K.

6.5. Radio Wave Attenuation due to Double Thermal Lenses

When the propagation path is intercepted by two thermal lenses, a considerable attenuation coefficient is observed from the simulation. For potassium content of 0.5% in the flame, attenuation coefficients were in the range of 1.53–0.33 dBm^{-1} over the region 12–22 m of wildfire plume (Fig. 12). An increase of potassium to 3% resulted in attenuation coefficient of magnitude of almost 10 times at the height of 12 m for a single thermal lens, thus attenuation coefficient was observed to be 1.65 dBm^{-1}. This is an increase of 0.12 dBm^{-1} from that due to a double lens with 0.5% potassium content in the flame. At a height of 22 m above ground, attenuation coefficient for a single lens increased by a factor of 2.4 to a value of 0.33 dBm^{-1}. According to the thermal lens model, a series of thermal lenses intercepting a UHF radio wave propagation path could lead to a considerable radio wave energy loss.

7. CONCLUSION

The effect of horizontal roll vortices and potassium content on the efficiency of radio wave communication on fire grounds can not be ignored. Numerical simulation show that when a horizontal vortex pair intercept propagation path of UHF signals, rays could be diverged from their propagation path by $1.24 - 6.82 \times 10^{-4}$ rads in plumes at normal wildfire temperatures (600–1300°C). This radio ray divergences occur at possible plant potassium content (i.e., 0.5–3.0%). The divergences are double when two horizontal vortices are considered. When simulated above vegetation canopy, thus in the region 12–22 m above ground, divergence was observed to range from 0.43–4.25 arcmins.

Attenuation coefficient due to up two horizontal vortices was observed to range from 0.136–1.65 dBm^{-1} for possible scenarios for the wildfire. The increase potassium concentration and number of thermal lenses increased radio attenuation coefficient markedly. The influence of potassium on the radio refractive index is a factor of the propagation frequency (as Eq. (45)). This could explain its little influence on dispersion at UHF.

ACKNOWLEDGMENT

We would like gratefully to acknowledge Staff Development Office of the University of Botswana for the financial support for this work. The work was partly supported by Emergency Management Australia under project No. 60/2001.

REFERENCES

1. Akhtar, K., E. J. Scharer, S. M. Tysk, and E. Kho, "Plasma interferometry at high pressures," *Review of Scientific Instruments*, Vol. 74, No. 2, 996–1001, 2003.
2. Bean, B. R. and J. E. Dutton, "Radio meteorology," *NBS Monogr.,* Vol. 92, 435, 1966.
3. Butler, C. J. and A. N. Hayhurst, "Kinetics of gas-phase ionization of an alkali metal, A, by the electron and proton transfer reactions: A + H_3O^+ → A + H_2O +H; AOH + AOH2+ H_2O in fuel-rich flames at 1800–2250 K," *J. Chem. Soc. Faraday Trans.,* Vol. 98, 2729–2734, 1998.
4. Burrows, W. G., "Distortion of a narrow radio beam in a convective medium," *AGARD Characteristics of the Lower*

Atmosphere Influencing Radio Wave Propagation, Vol. 21, N84–24943, 15–32, 1984.

5. Butler, B. W., J. Cohen, D. J. Latham, R. D. Schuette, P. Sopko, K. S. Shannon, D. Shannon, and L. S. Bradshaw, "Measurements of radiant emissive power and temperatures," *Crown Fires. Can. J. For. Res.,* Vol. 34, No. 8, 1577–1587, 2004.
6. Carter, E. and B. Milton, "Internal combustion engine performance in the fire ground," *International Journal of Wildland Fire,* Vol. 4, No. 2, 83–91, 1994.
7. Catchpole, W. R., E. A. Catchpole, A. G. Tate, B. W. Butler, and R. C. Rothermel, "A model for the steady spread of fire through a homogeneous fuel bed," *Proceedings of 4th International Conference on Forest Fire Research: 2002 Wildland Fire Safety,* X. Viegas edition, 106, Luso Coimbra, Portugal, Millpress, Rotterdam, November 18–23, 2002.
8. Church, C. R., J. T. Snow, and J. Dessens, "Intense atmospheric vortices associated with 1000 MW fire," *Bulletin of the American Meteorological Society,* Vol. 61, 682–694, 1980.
9. Clark, T. L., M. Griffiths, M. J. Reeder, and D. Latham, "Numerical simulations of grassland fires in the northern territory, Australia, A new subgrid-scale fire parameterization," *Journal of Geophysical Research,* 108 D18, 4589, ACL 14-1–14-15, 2003.
10. Clark, T. L., M. J. Reeder, M. Griffiths, D. Packham, and N. Krusel, "Infrared observations and numerical modelling of grassfires in northern territory, Australia," *Meteorology and Atmospheric Physics,* Vol. 88, 193–201, 2005.
11. Cruz, M. G., B. W. Butler, M. E. Alexander, J. M. Forthofer, and R. H. Wakimoto, "Predicting the ignition of crown fuels above a spreading surface fire Part I: Model idealization," *International Journal of Wildland Fire,* Vol. 15, 47–60, 2006.
12. Frankenberg, E., D. Mckee, and D. Thomas, "Health consequences of forest fires in Indonesia," *Demography,* Vol. 42, No. 1, 109–129, 2002.
13. Frost, L. S., "Conductivity of seeded atmospheric pressure plasmas," *Journal of Applied Physics,* Vol. 32, No. 10, 2029–2036, 1961.
14. Gill, A. M., P. H. R. Moore, and R. J. Williams, "Fire — weather in wet-dry tropics of the world heritage Kakadu National Park, Australia," *Australian Journal of Ecology,* Vol. 21, 302–308, 1996.
15. Gossard, E. E., "Refractive index variance and its height distribution in different air masses," *Radio Science,* Vol. 12, 89–

105, 1977.

16. Haines, D. A., "Horizontal roll vortices and crown fires," *Journal of Applied Meteorology,* Vol. 21, 751–763, 1982.
17. Haines, D. A. and M. C. Smith, "Three types of horizontal vortices observed in wildland mass and crown fires," *Journal of Applied Meteorology,* Vol. 26, 1624–1637, 1987.
18. Heilman, W. E., "Atmospheric simulations of extreme surface heating episodes on simple hills," *International Journal of Wildland Fire,* Vol. 2, No. 3, 99–114, 1992.
19. Heilman, W. E. and J. D. Fast, "Simulations of horizontal roll vortex development above lines of extreme surface heating," *International Journal of Wildland Fire,* Vol. 21, 751–763, 1992.
20. Jenkins, A., "Investigating the haines index using parcel model theory," *International Journal of Wildland Fire,* Vol. 13, 297–309, 2004.
21. Koalaga, Z., "Determination of equilibrium composition of CxHyOzNt plasmas out of thermodynamic equilibrium," *Eur. Phys. Journal D.,* Vol. 17, 235–247, 2001.
22. Koppman, R., K. von Czapicwski, and J. S. Reid, "A review of biomass emissions, Part I : Gaseous emissions of carbon monoxide, methane, volatile organic compounds and nitrogen containing compounds," *Atoms. Chem. Phys. Discuss,* Vol. 5, 10455–10516, 2005.
23. Latham, D., "Space charge generated by wind tunnel fires," *Atmospheric Research,* Vol. 51, 267–278, 1999.
24. Marcelli, T., P. A. Santoni, A. Simeoni, E. Leoni, and B. Porterie, "Fire spread across pine needle fuel beds: characterization of temperature and velocity distribution within the fire plume," *International Journal of Wildland Fire,* Vol. 13, 37–48, 2004.
25. Mecer, G. N. and R. O. Weber, "Plumes above line fires in a cross wind," *Int. Journal of Wildland Fire,* Vol. 4, No. 4, 201–207, 1994.
26. Nikolaenko, A. and G. Ahlers, "Nusselt number measurements for turbulent rayleigh-bernard convection," *Physical Review Letters,* Vol. 9, No. 8, 1–4, 2003.
27. Okuno, T., N. Sonoyama, J. Hayashi, C. Li, C. Sathe, and T. Chiba, "Primary release of Alkali and Alkaline earth metallic species during pyrolysis of pulverized biomass energy and fuels," Vol. 19, 2164–2171, 2005.
28. Palmer, T. Y., "Visible, infrared (IR) and microwave propagation in and near large fires," *SPIE Atmospheric Effects on System Performance,* Vol. 35, 1981.

29. Porterie, B., J. C. Loraud, D. Morvan, and M. Larini, "A numerical study of buoyant plumes in cross-flow conditions," *International Journal of Wildland Fire,* Vol. 10, 137, 1999.
30. Radojevic, M., "Chemistry of forest fires and regional haze with emphasis on Southeast Asia," *Pure and Applied Geophysics,* Vol. 12, 157–187, 2003.
31. Raison, R. J., P. K. Khaina, and P. Woods, "Mechanisms of element transfer to the atmosphere during vegetation burning," *Canad. Journal of Forest Res.,* Vol. 15, 132–140, 1985.
32. Sanchez, O., D. J. Raymond, L. Libersky, and A. G. Petschek, "The development of thermals from rest," *Journal of the Atmospheric Sciences,* Vol. 46, 2280–2292, 1989.
33. Stronach, N. R. H. and S. J. Mc Naughton, "Grassland fire dynamics in serengeti ecosystem and potential method of retrospectively estimating fire energy," *Journal of Applied Ecology,* Vol. 26, No. 3, 1025–1033, 1989.
34. Tapper, N. J., G. Garden, J. Gill, and J. Fernon, "The climatology and meteorology of high fire danger in northern territory," *Rangeland Journal,* Vol. 15, No. 2, 339–351, 1993.
35. Weber, R. O., A. M. Gill, P. R. A. Lyons, and G. N. Mercer, "Time dependence of temperature above wildland fires," *CALM Science,* Vol. 4, 17–22, 1995.
36. Westberg, H. M., M. Bystrom, and B. Lecker, "Distribution of potassium, chlorine and sulphur between solid and vapour phases during combustion of wood and coal," *Energy and Fuels,* Vol. 17, 18–28, 2003.
37. Williams, D. W., J. S. Adams, J. J. Batten, G. F. Whitty, and G. T. Richardson, "Operation euroka: an Australian mass fire experiment," Report 386, Defense Standards Laboratory, Maribyrnor, Victoria Australia, 1970.
38. Williams, R. P., R. A. Congdon, A. C. Grice, and P. J. Clarke, "Effect of fire regime on plant abundance in tropical eucalypt savanna of north-eastern Australia," *Austral Ecology*, Vol. 28, 327–338, 2003.
39. Ventura, J. M. P. and F. M. C. Rego, "Modelling the shape of temperature-time curves," *13th Fire and Forest Meteorology Conference*, Lorne, Australia, 1996.
40. Viegas, D. X., "Fire behaviour and fire line intensity," *Ann. Medit. Burns Club,* Vol. 6, No. 3, 179–186, 1993.
41. Viegas, D. X., "Forest f propagation," *Phil. Trans. R. Soc. Lond. A.,* Vol. 356, 2907–2928, 1998.

42. Vodacek, A., R. L. Kremens, S. C. Fordham, S. C. VanGorden, D. Luisi, J. R. Schott, and D. J. Latham, "Remote optical detection of biomass burning using potassium emission signature," *Int. Journal of Remote Sensing,* Vol. 23, 2721–2726, 2002.
43. Yamasoe, M. A., P. Artaxo, A. H. Miguel, and A. G. Allen, "Chemical composition of aerosol particles from direct emissions of vegetation fires in the Amazon Basin: wate-soluble species and trace elements," *Atmospheric Environment,* Vol. 34, 1641–1653, 2000.
44. Potter, B. E., "A dynamics based view of Atmospheric-fire interactions," *Int. Journal of Wildland Fire*, Vol. 11, 247–255, 2002.
45. Oliveira, L. A., D. X. Veigas, V. Vareli, and A. M. Raimudo, "On the soil thermal effect under the surface fire conditions," *Proceedings of 2nd Int. Conf. Forest Fire Research*, Vol. III, D03, 833–847, Coimbra, 2002.
46. Haines, D. and L. J. Lyon, "Horizontal roll vortices in complex terrain," *Fire Management Today*, Vol. 51. No. 2, 15–17, 1990.
47. Kulemin, G. P. and V. B. Razskazovsky, "Radar reflections from explosions and gas wake of operting engine," *IEEE Transactions on Antennas and Propagation*, Vol. 45, No. 4, 731–739, 1997.
48. Kuei-Chaio, K., "Theory of Raman intensities of diatomic molecule," *Chinese Journal of Physics*, Vol. 8, No. 2, 58–63, 1970.